Ion acceleration in Ar–Xe and Ar–He plasmas. II. Ion velocity distribution functions

Ioana A. Biloiu[a] and Earl E. Scime
Department of Physics, West Virginia University, Morgantown, West Virginia 26506, USA

(Received 3 August 2010; accepted 6 October 2010; published online 9 November 2010)

Ion velocity distribution functions (ivdfs) are investigated by laser induced fluorescence in Ar–Xe and Ar–He expanding helicon plasmas as a function of gas composition. In the case of Ar–Xe plasma, it was found that in the helicon source, both the Ar^+ and Xe^+ vdfs are unimodal. Their parallel speeds are subsonic and unaffected by changes in gas composition. At the end of the source, the argon ivdf shows a bimodal structure indicative of an electric double layer upstream of the measurement location. The fast argon ion component parallel velocity increases with Xe fraction from 6.7 to 8 km/s as the Xe fraction increases from 0% to 4%. In the expansion region, the bimodal character of Ar ivdf is maintained with a supersonic fast component reaching parallel speeds of 10.5 km/s. For all the studied plasma conditions and different spatial locations, the Xe^+ vdf exhibits a unimodal structure with a maximum parallel flow velocity of 2.2 km/s at the end of the source. For Ar–He plasma, the Ar ivdf is bimodal with the fast ion component parallel velocity increasing from 5.2 to 7.8 km/s as the He fraction increases from 0% to 30%. For the same He fraction range, the slow argon ion population distribution changes from a single Gaussian to a wide distribution extending all the way from the speed of the fast population to 0 m/s. © *2010 American Institute of Physics*. [doi:10.1063/1.3505823]

I. INTRODUCTION

It has been shown elsewhere[1–3] that for argon plasma in the HELIX-LEIA helicon source-expansion chamber system, an electric double layer (EDL) forms below a threshold pressure of 1–2 mTorr. EDL is oriented with a high potential side toward HELIX and a low potential side toward LEIA. The EDL potential drop and the magnetic field expansion produce ion acceleration that results in a bimodal Ar^+ ion velocity distribution function (ivdf) downstream of the EDL. Laser induced fluorescence (LIF) measurements of the parallel argon ion velocity distribution function revealed that the EDL is located just upstream of the HELIX-LEIA junction, where the magnetic field gradient is a maximum. As with a plasma sheath, ions have to enter the EDL from the plasma at the Bohm speed. For single ion component plasmas, the Bohm velocity is set by the electron temperature. For bi- or multicomponent plasmas, the Bohm velocity depends on the relative ion densities and the electron temperature. The work reported here examines how the EDL formation, strength, and location are influenced by mixing the primary neutral gas (Ar) with heavier gas (Xe) or lighter gas (He).

In the companion paper,[4] referred to as Part I throughout this paper, we described the changes in the electron distribution functions, ion production, and plasma composition in Ar–Xe and Ar–He plasmas as a function of the filling fractions of heavier and lighter gas species. In this work, we report the changes in the ivdf as a function of plasma composition under identical operating conditions as in Part I. The lack of a suitable LIF scheme for He ions prevented us from directly examining the He^+ velocity distribution.

[a]Author to whom correspondence should be addressed. Electronic mail: iabiloiu@yahoo.com.

II. LASER INDUCED FLUORESCENCE DIAGNOSTICS

A. LIF principles and basic hardware

A detailed discussion of one- and two-dimensional laser induced fluorescence principles of operation, analysis methodology, and experimental apparatus is provided in Ref. 5. Therefore, we only provide a brief review of LIF. In a typical LIF measurement, the particle ensemble velocity distribution function (vdf) is obtained by scanning the laser frequency over the range of interest and recording the fluorescence spectrum. For a three-level LIF scheme, when the incident photon has an appropriate frequency in the particle's rest frame, a particular quantum level, usually a metastable state, is optically pumped and the population of an upper quantum level increases. The upper level then spontaneously decays to a third level by emitting a photon. The intensity of the fluorescence radiation as a function of laser frequency is a direct measurement of the initial state vdf, although processes such as Zeeman splitting may have to be included in the analysis of the data to determine the particle velocity distribution function. The measured vdf only contains one-dimensional velocity information since the measurement is the projection of the three-dimensional vdf on the laser propagation direction. For example, when the laser is injected along the x axis, the measured $f(v_x)$ is an average over the distributions along the two directions orthogonal to $\boldsymbol{x}$,

$$f(v_x) = \int \int f(v_x, v_y, v_z) dv_y dv_z. \quad (1)$$

The determination of the average particle velocity and temperature from the LIF measurement is straightforward: v_x is found from the peak in the measured $f(v_x)$ versus laser frequency[6]

$$v_x \cong \lambda_0 \Delta\nu_{\text{total}}, \tag{2}$$

where the velocity v_x is in m/s if the rest frame wavelength λ_0 is in nanometer and the frequency shift $\Delta\nu_{\text{total}}$ (which generally includes Zeeman corrections) is in gigahertz. Because the laser bandwidth is much narrower than the particle vdf, the high velocity resolution (~50–100 m/s) is achievable.[7] The temperature is obtained from the full width at half-maximum (FWHM) of the fluorescence line, assuming that Doppler broadening dominates over other line-broadening mechanisms (Stark broadening, power broadening, and instrumental broadening) and the natural linewidth of the absorption line

$$k_B T_x = (m_p/8 \ln 2)(\Delta v_x)_{1/2}^2, \tag{3}$$

where m_p is the particle mass, $(\Delta v_x)_{1/2}$ is the FWHM of the velocity distribution, and k_B is the Boltzmann's constant.

The LIF experimental setup consists of a 100 MHz linewidth, continuous wave Ar ion-pumped dye laser (Coherent 899) that pumps transitions in both Ar^+ ($3d\ ^2G_{9/2} \rightarrow 4p\ ^2F^0_{7/2}$ at 611.661 nm) and Xe^+ ($5d\ ^4D_{7/2} \rightarrow 6p\ ^4P_{5/2}$ at 605.278 nm). The laser system includes a high resolution wavemeter (Burleigh WA-1500) for coarse tuning and wavelength monitoring. After passing through a beam splitter, the laser beam is modulated with an optical chopper at few kHz and then coupled into a multimode, nonpolarization preserving, optical fiber. 10% of the laser beam is extracted before the optical chopper and passed through an iodine cell for a consistent zero velocity reference. Appropriate iodine lines are used as a zero velocity reference for the LIF measurements.[8,9] Light from the collection optics passes through a 1 nm bandpass interference filter centered at 461 nm for Ar^+ (530 nm for Xe^+). Following the filter is a photomultiplier detector (PMT) with an integrated 30 kHz bandwidth preamplifier. A lock-in amplifier (Stanford Research 830), referenced to the chopper, is used to isolate the LIF signal from background emission at the fluorescence wavelength. The injected laser power density of ~10 mW/mm^2 ensures that the laser optical pumping is in a linear regime, i.e., the LIF signal is proportional to the laser intensity and LIF saturation effects are avoided.[10–12]

B. Argon ion LIF

For Ar^+ LIF, the classic Ar^+ three-level LIF scheme was used.[13] The Ar^+ $3d\ ^2G_{9/2}$ metastable state is optically pumped by 611.6616 nm (vacuum wavelength) laser light to the $4p\ ^2F^0_{7/2}$ state, which then decays to $4s\ ^2D_{5/2}$ state by emission at 461.086 nm. Since the first state is metastable, the homogenous linewidth of the absorption process is dominated by the natural linewidth of the $4p\ ^2F^0_{7/2}$ level. The resultant 1.9×10^{-2} GHz linewidth is infinitely small compared to typical Doppler broadened linewidths for Ar^+ (approximately 1 GHz at room temperature).[14] The interaction between the magnetic moment of the electronic states and an external magnetic field leads to Zeeman splitting of spectral lines. For our argon ion LIF pump line ($3d\ ^2G_{9/2} \rightarrow 4p\ ^2F^0_{7/2}$), the Zeeman splitting of the $\Delta M_J = \pm 1$ transitions leads to $\sigma^{\pm}$ clusters (each of them consisting of eight lines) symmetrically shifted from the original wavelength. Their shift is proportional to the magnetic field strength (1.52 GHz/kG), and is therefore ignorable for the weak magnetic field in LEIA. The $\Delta M_J = 0$ transitions lead to an unshifted π cluster of lines. For the Ar^+ 611.6616 nm (16 348.91 cm^{-1}) absorption line, the closest iodine line with a sufficient intensity is the 16 348.94 cm^{-1} line. The difference of 1.08 GHz between the iodine line and the 611.6616 nm argon ion line is subtracted from each flow calculation.

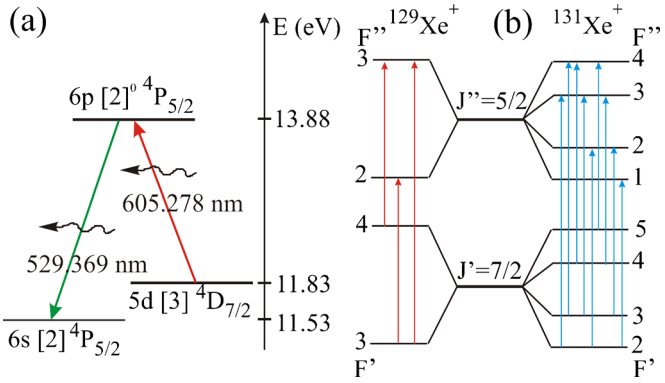

FIG. 1. (Color online) (a) Three-level Xe^+ LIF scheme and (b) hyperfine structure of 605.278 nm line of the odd isotopes due to nuclear spin splitting.

C. Xenon ion LIF

In the three-level Xe^+ LIF scheme [see Fig. 1(a)], the laser wavelength is tuned to 605.2781 nm to pump Xe^+ from the metastable state $5d\ ^4D_{7/2}$ to the excited state $6p\ ^4P_{5/2}$. Ions from $6p\ ^4P_{5/2}$ state decay to $6s\ ^4P_{5/2}$ state, emitting a 529.369 nm photon. In the case of Xe^+, the hyperfine splitting is significant and thus the absorption line shape in Xe^+ LIF is a convolution of the hyperfine splitting and Doppler broadening. The hyperfine structure of Xe^+ is a nuclear effect and includes the effects of mass (isotope effect) and nuclear spin (caused by the coupling between the nuclear spin **I** and the total electronic angular momentum **J**). Xenon has a rich spectrum of isotopes, five of them having natural abundances of 10% or more. Each of these isotopes causes a shift of the energy levels—the isotopic splitting—involving a transition of a few tens of MHz. Of the nine isotopes of xenon, seven have an even atomic mass. Thus, they have a nuclear spin of $\mathbf{I}=0$ and do not contribute to the nuclear-spin splitting. The remaining two isotopes have odd atomic masses and nonzero nuclear spin quantum numbers **I**. The lighter isotope, $^{129}Xe^+$ has $I=1/2$ and $^{131}Xe^+$ has $I=3/2$. These nonzero nuclear spins cause nuclear spin splitting of the energy levels [see Fig. 1(b)]. This nuclear-spin splitting is considerably larger than the isotopic splitting and is responsible for most of the characteristic shape of the $5d\ ^4D_{7/2} \rightarrow 6p\ ^4P_{5/2}$ line.[15] In the case of weak to moderate external magnetic field strengths, the hyperfine structure is further split in $2F+1$ sublevels. For instance, Zeeman splitting for the $F'=3 \rightarrow F''=2$ transition for $^{129}Xe^+$ and $^{131}Xe^+$ yields four π-lines for which $\Delta M_F = 0$ and ten σ-lines for which $\Delta M_F = \pm 1$. A complete analysis of an Xe^+ LIF measurement

requires accounting for Doppler broadening as well as the hyperfine, isotopic, and possibly Zeeman structures of the $5d\ ^4D_{7/2} \rightarrow\ 6p\ ^4P_{5/2}$.[16]

The identification and analysis of iodine lines was performed for the Xe^+ LIF scheme. The most intense iodine line in the relevant wavelength range is at 16 521.45 cm^{-1}. Available tables[17,18] based on early measurements by Humphreys[19] provide a value for the Xe^+ transition wave number of 16 521.22 cm^{-1}. Based on interferometric measurements in a later paper,[20] Humphreys reported an improved value of 16 521.285 cm^{-1}. Hansen and Persson[21] also reported a wave number of 16 521.22 cm^{-1}. The most recent wave number measurements are by Cedolin *et al.*[22] who reported a value of 16 521.23 cm^{-1} based on a direct and reflected laser induced fluorescence and by Sadeghi *et al.*[23] who reported a wave number value of 16 521.299 cm^{-1} based on Lamb dip spectroscopy. Converted into frequency, the variation between maximum and minimum reported wave number values (~0.08 cm^{-1}) spans 2.4 GHz. In terms of ion speed, this uncertainty corresponds to an unacceptably large speed uncertainty of ~1.5 km/s. Therefore, measurements of perpendicular Xe^+ ivdf on the LEIA axis were used to obtain an absolute zero velocity reference wave number of 16 521.332 cm^{-1}. The frequency difference between the reference iodine line and the rest frame Xe^+ 605.2781 nm absorption line is therefore 3.91 GHz. Due to the isotopic composition of natural xenon and the presence of a nonzero nuclear spin in odd isotopes 129 and 131, the absorption spectrum of Xe^+ spreads over approximately 8 GHz and interpretation is much more difficult than for argon. The 3.91 GHz zero velocity frequency correction is applied to the peak of the measured distribution (associated with ^{132}Xe isotope due to its highest abundance of 27%). Because the xenon ion level splitting in nineteen individual hyperfine lines is asymmetric, the LIF measured Xe^+ line shape is non-Gaussian. It is worth noting that in contrast to the argon measurements, the Xe^+ ion temperature cannot be uniquely determined.

III. ION ACCELERATION IN TWO-ELECTROPOSITIVE GAS SPECIES PLASMAS

The combined effects of the electric double layer potential drop and magnetic field expansion produce ion acceleration that results in a bimodal Ar ion velocity distribution function downstream of the EDL at the end of helicon sources.[24–26] Retarding the field energy analyzer and LIF measurements of the parallel argon ivdf revealed that EDL is located at the spatial position where the magnetic field gradient is a maximum.[27,28] For the HELIX-LEIA system, the EDL forms just upstream of the chamber junction. To demonstrate EDL formation (if any) in Ar–Xe and Ar–He mixed plasmas, and the influence (if any) of a heavier and, respectively, lighter gas species on probe ion acceleration, the parallel ion velocity distribution function of argon and xenon ions was measured as a function of plasma composition at three spatial locations: in the source upstream the junction at $z=126$ cm, in the source in the vicinity of the junction at $z=146$ cm, and downstream of the chamber junction at $z=169$ cm. For these studies, the laser light was injected along the HELIX axis from the end of the plasma source. The LIF signal was gathered with collection optics mounted on radially viewing windows at $z=126$ and 146 cm [see Fig. 1(a) in Part I]. For LIF measurements in the expansion region at $z=169$ cm, a scanning internal probe was used. Detailed descriptions of the LIF injection and detection systems can be found in Ref. 5.

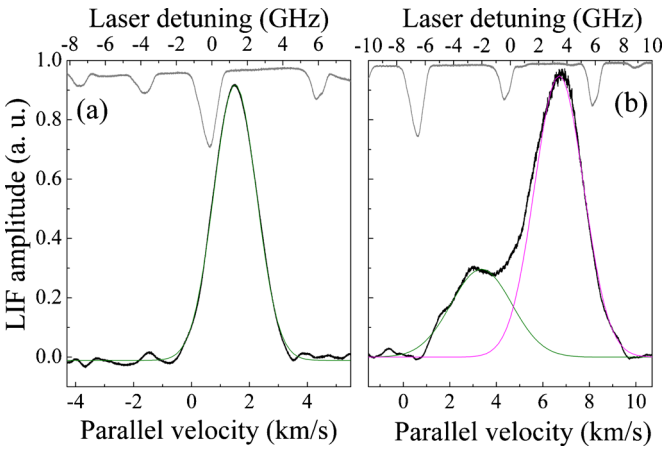

FIG. 2. (Color online) Argon ion parallel velocity distribution functions in (a) HELIX at $z=126$ cm and (b) HELIX at $z=146$ cm. The thick black lines are LIF signals; the thin lines are Gaussian fits assuming a single and a dual ion population line; and at the top is the iodine reference spectrum. The ivdf evolves from unimodal at $z=126$ cm into bimodal at $z=146$ cm.

A. Ar^+ vdf in Ar–Xe plasma

For the LIF investigations, the same source parameters as for the Langmuir probe and optical emission spectroscopy (OES) studies presented in Part I were used. Discharges in pure Ar, Xe, or their mixtures were obtained for 750 W of input rf power. Since the rf energy coupling to the plasma varied from one gas composition to the other, the matching network tuning for minimum reflected power was performed for each discharge condition. During the operation, the reflected rf power was monitored in real time and maintained below 20 W, i.e., less than 3% of the forward rf power. The rf driving frequency was set to 9.5 MHz for which quiescent and stable plasma over prolonged periods and for a wide range of Ar/Xe mixture ratios could be maintained. As in the EEDF and OES measurements, the HELIX magnetic field strength was 700 G and the LEIA magnetic field strength was 10 G. The gas composition was varied by modifying the individual argon and xenon mass flow rates while maintaining a constant 10 (SCCM) (SCCM denotes standard cubic centimeters per minute at STP) total mass flow rate.

1. Effect of Ar/Xe ratio on Ar^+ vdf in the plasma source

A typical parallel Ar ivdf on the axis of the source at $z=126$ cm is shown in Fig. 2(a). On the high potential side of an electric double layer, ion species enter either with their individual Bohm speeds[29–31]

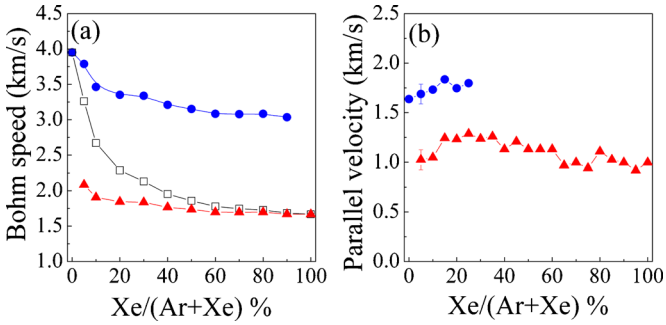

FIG. 3. (Color online) (a) Individual ion sound speeds (circles for Ar^+ and triangles for Xe^+) and the system sound speed (open squares) as function of xenon fraction in HELIX at $z=126$ cm. (b) Parallel ion flow speeds in HELIX at $z=126$ cm vs xenon fraction (same symbol assignment).

$$c_{\mathrm{Ar+,Xe+}} = \sqrt{\gamma k_B T_e / M_{\mathrm{Ar,Xe}}}, \tag{4}$$

where $\gamma=1$ for isothermal expansion or the system Bohm speed

$$c_{\mathrm{system}} = [(n_{\mathrm{Ar+}}/n_e)c_{\mathrm{Ar+}}^2 + (n_{\mathrm{Xe+}}/n_e)c_{\mathrm{Xe+}}^2]^{1/2}. \tag{5}$$

Since the electron temperature and Xe and Ar ion densities vary with xenon fraction [see Fig. 4(a) in Part I], the individual and system ion sound speeds also vary. Figure 3(a) shows the computed Bohm speeds at $z=126$ cm in HELIX, 24 cm upstream of the HELIX-LEIA junction, based on Langmuir probe measurements and the ion density model presented in Part I. The argon and xenon individual ion sound speeds are the largest in the pure argon plasma. These slightly decrease with the increasing xenon fraction. The system ion sound speed follows the trend in electron temperature and sharply decreases with the xenon fraction from the argon ion sound speed ($c_{\mathrm{Ar+}}=4$ km/s) in pure argon plasma to the xenon ion sound speed ($c_{\mathrm{Xe+}}=1.7$ km/s) in pure xenon plasma. The largest change in system ion sound speed occurs as the xenon fraction changes from 0% to 25%.

The experimentally determined parallel ion flow velocities for argon and xenon ions at the same spatial location in HELIX ($z=126$ cm) versus xenon fraction are shown in Fig. 3(b). The measured speeds are much lower than the individual ion sound speeds and are independent of xenon fraction, suggesting that the EDL (if present) is located further downstream than the measurement location. Since the ratio of the argon to xenon speed is approximately constant at 1.7 and consistent with $\sqrt{M_{\mathrm{Xe}}/M_{\mathrm{Ar}}} \cong 1.8$, these measurements suggest the presence of a slight axial potential gradient that accelerates argon and xenon ions to speeds in a manner inversely proportional to the square root of their masses (as would be expected for an axial electric field).

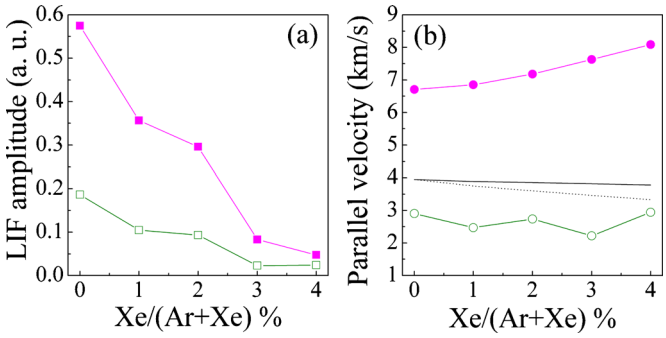

FIG. 4. (Color online) At $z=146$ cm in HELIX, the Ar^+ LIF amplitude (a) and parallel flow speed (b) as function of small changes in the xenon fraction. Filled and open symbols denote the fast and slow ion group, respectively. (b) The Ar^+ (solid line) and system (dotted line) sound speeds calculated based on measurements at $z=126$ cm.

The measured argon LIF signal, and by implication the Ar^+ metastable population, decreases with increasing xenon fraction until the signal completely disappears for xenon concentrations greater than 25%. This is consistent with the 2 eV decrease in electron temperature and the calculated 76% decrease in the Ar^+ density [see Figs. 4(a) and 6(a) in Part I]. In other words, the Ar^+ ground state population is too small and there are not enough high-energy electrons to populate the $3d\ ^2G_{9/2}$ ion metastable level located 19.11 eV above the argon ion ground level.[32] Conversely, the Xe^+ LIF signal shows a gradual increase with xenon fraction consistent with the increase in Xe^+ population as the Xe fraction is increased [see Fig. 6(a) in Part I]. The Ar ion temperature slightly increases from ~0.15 eV for pure Ar plasma to ~0.22 eV for 75%Ar/25%Xe plasma.

Further downstream at $z=146$ cm in HELIX (4 cm upstream of the HELIX-LEIA junction), the bimodal argon ivdfs [see Fig. 2(b)] are observed in Ar–Xe plasmas. At this position, the fast Ar^+ LIF amplitude dramatically decreases (more than a factor of 10) with the increasing xenon fraction, entirely disappearing for xenon fractions greater than 4% [see Fig. 4(a)]. Since at $z=126$ cm the Ar^+ LIF signal is detectable up to xenon fractions of ~20% and for xenon fractions of 0 to 4% the total pressure and the electron temperature are relatively constant, the change in Ar^+ density with the increasing xenon fraction appears to be highly nonuniform along the HELIX axis.

The argon ivdfs are similar to those found in pure argon plasma with the fast group having a parallel velocity of 6.7 km/s at 0% xenon fraction slightly increasing to 8 km/s at 4% Xe. The slow group velocity is roughly constant at ~3 km/s. The increase in parallel argon ion velocity between $z=126$ and 146 cm is equivalent to an increase in parallel kinetic energy from 0.7 to 9.4 eV. This gain in parallel kinetic energy cannot be fully explained by the conversion of upstream perpendicular energy into downstream parallel kinetic energy due to magnetic moment conservation (at $z=146$ cm the magnetic field lines are no longer parallel but are slightly divergent). Another possibility could be the conversion of azimuthal flow kinetic energy into parallel flow energy. However, the magnetic moment conservation and the available flow kinetic energy could only provide at most a 2 eV change in energy.[25] Therefore, a localized electric field between these two locations is implied. Unfortunately, the geometry of HELIX does not permit probe measurements at this location. Assuming that the electron temperature does not vary much over 20 cm, a rough estimate of the individual and system ion speeds [see Fig. 4(b)] based on the electron temperature and density measurements at $z=126$ cm (6.5 eV and 1.08×10^{11} cm^{-3}) shows that at $z=146$ cm, the fast ion group is supersonic ($\sim 1.7 c_{\mathrm{Ar+}}$); consistent with an EDL

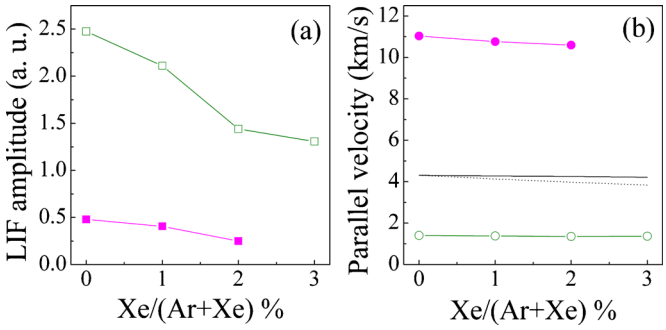

FIG. 5. (Color online) (a) Ar^+ LIF amplitude and (b) parallel flow speed as function of xenon fraction at $z=169$ cm in LEIA. Filled and open symbols denote the fast and slow ion groups, respectively. (b) The Ar^+ (solid line) and system (dotted line) sound speeds calculated based on measurements at $z=169$ cm.

somewhere between $z=126$ and 146 cm. Previous experiments have shown that in pure argon plasmas, a decrease in the downstream Ar^+ density often corresponds to an increase in the potential difference across the EDL.[7] Therefore, these measurements may be indicative of modest changes in the strength of the EDL as the xenon fraction increases from 0% to 4%.

The LIF collection optics mounted at $z=146$ cm is capable of scanning a few centimeters along the HELIX axis. The argon ion beam velocities at $z=147$ and 148 cm exhibit the same dependence on xenon fraction as the $z=146$ cm measurements, i.e., an increase of ~1 km/s over a 4% change in xenon fraction. This slight but monotonic increase (~2% and ~5% at $z=147$ and 148 cm, respectively) in the parallel flow velocity is consistent with the parallel acceleration expected for magnetic field divergence effects.

2. Effect of Ar/Xe ratio on Ar^+ vdf in the expansion region

Ar^+ LIF measurements as a function of xenon fraction were obtained in LEIA with the scanning probe at $z=169$ cm. The bimodal character of the argon ivdf observed in HELIX just upstream of the HELIX-LEIA junction is also observed in LEIA.[33] As shown in Fig. 5(a), similar to what was observed in HELIX, the LIF intensity of the fast

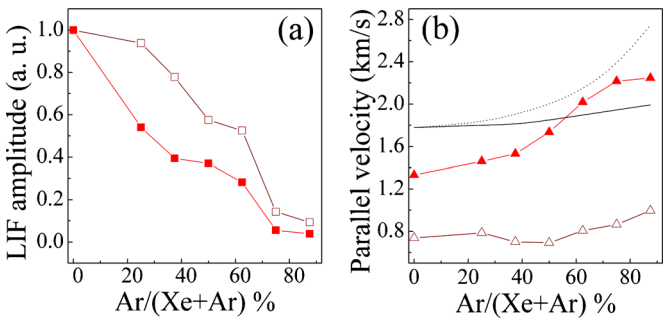

FIG. 6. (Color online) (a) Normalized Xe^+ LIF amplitude and (b) Xe^+ parallel flow speed at $z=126$ cm (open symbols) and $z=146$ cm (filled symbols) in HELIX vs argon fraction, respectively. Also shown in (b) are the Xe^+ (solid line) and system (dotted line) sound speeds based on local measurements.

Ar^+ population decreases with xenon fraction and completely disappears for xenon fractions greater than 3% (in HELIX the signal disappeared for xenon fractions greater than 4%). Since the LIF detection system in LEIA is different than in HELIX, direct comparison of LIF signal amplitudes is inappropriate. However, the relative values do provide some insight into the dependence of the fast and slow ion populations on the xenon fraction. At the end of HELIX, the fast ion population LIF signal is much larger than the slow ion population LIF signal [see Fig. 4(a)]; 75% of the total population for pure argon and 81% of the total population for a 3% xenon fraction. In LEIA the fast ion population is a small fraction of the total ion population: 15% for pure argon and only 4% for a 3% xenon fraction. These observations are consistent with different origins of the two ion populations observed in LEIA: the slow ions are a background ion population locally created and the fast ions are an ion population created upstream in the source and subsequently accelerated into the LEIA chamber. Under these assumptions, the decrease in the fraction of the fast ion population at $z=169$ cm is entirely consistent with a metastable quenching of the fast ion population. Since LIF only detects ions in the 3d $^2G_{9/2}$ metastable state, only a small fraction of the fast ion population is detectable by LIF. Taking the upper limit of the quenching cross-section for collisions of the 3d $^2G_{9/2}$ state with ground state neutral argon to be 1×10^{-14} cm^2,[34] the resultant mean free path (mfp) is ~17 cm, one and a half times the distance between the likely EDL location and observation point in LEIA. Thus, only ~20% of the fast ions in the 3d $^2G_{9/2}$ metastable state accelerated by the EDL at the end of HELIX will survive and be detected in LEIA. The effect of metastable quenching on LIF measurements of ion beams was recently demonstrated in a series of combined RFEA and LIF experiments in LEIA.[35] The decrease in LIF signal with the increasing xenon fraction results from fewer argon ions in the 3d $^2G_{9/2}$ metastable state being generated in the source (recall that an increasing xenon fraction depletes the eedf of higher energy electron and thereby reduces the rate of argon ion metastable creation). Although the cross-sections for Ar^{+*}–Xe quenching collisions are unknown, they are probably negligible for such small xenon fractions. It is interesting to note that plasma expansion leads to the cooling of the slow ion population distribution. At the end of the source the argon ion temperature is ~0.35 eV, whereas in the expansion region, it is 0.17 eV, which is independent of the slight 3%–4% change in the gas composition.

As shown in Fig. 5(b), the parallel flow speed of the fast population in LEIA is larger (~10.8 km/s) than the parallel flow speed at the end of HELIX (~8 km/s). Conversely, the parallel flow speed of the slow population (1.4 km/s) is smaller than the corresponding HELIX value of 2.5 km/s. Based on electron temperature and electron density measurements at this location (~7 eV and $\sim2.1\times10^9$ cm^{-3}), the calculated Bohm speed is roughly constant ~4.2 km/s. The parallel flow speeds of both fast and slow ion populations in LEIA are unaffected by the small change in xenon fraction. A parallel ion flow speed of 10.8 km/s in LEIA corresponds to a parallel kinetic energy of ~24 eV. Given the ~13 eV (8 km/s) kinetic energy measured at the end of HELIX, these

measurements suggest that the ions gain an additional ~11 eV as they travel through the divergent magnetic field region from $z=146$ cm (HELIX) to $z=169$ cm (LEIA). Consistent with this interpretation is the observation that for small changes in the xenon fraction (0%–4%) the plasma potential in LEIA is roughly constant [Fig. 6(b) in Part I], i.e., there is no change in the total potential drop across the EDL (unfortunately, measurement of the plasma potential just upstream the EDL is not possible in the HELIX-LEIA system but based on Ar^+ LIF measurements in HELIX and the energy balance equation the estimated upstream plasma potential is ~43–46 V for these conditions, ~10 V larger than at the $z=126$ cm position). Note also that the magnetic field ratio was held constant in these experiments. Thus, it appears that a small addition of xenon to argon plasma in the range of pressure where the EDL is present does not alter the parallel speed of the supersonic ($\sim 2.6\ c_{Ar+}$) fast ion group and that the total energy gain arises from a combination of acceleration in the EDL ($12-14\ \text{eV} \cong 2k_B T_e$) and adiabatic expansion in the divergent magnetic field (~11–13 eV).

B. Xe^+ vdf in argon-xenon plasma

To examine the effect of light ion mass doping, LIF measurements of the xenon ivdf were obtained as a function of argon fraction in HELIX at $z=126$ and 146 cm. The plasma conditions were the same as for the xenon fraction experiments except the total mass flow rate was maintained at 8 SCCM; EDL formation is more easily triggered at lower pressures.[36] The total neutral pressure in HELIX decreased from 1.3 mTorr for 0% Ar to 1.1 mTorr for 87% Ar. For argon fractions less than 80%, the ion density was dominated by the xenon ion [see Fig. 6(a) in Part I]. Since the Xe^+ $5d\ ^4D_{7/2}$ metastable state formation is dominated by electron collisions with the Xe^+ in the ground state, the LIF signal is proportional to the electron density, the xenon neutral density, and the Xe^+ density. As can be seen in Fig. 6(a) at both $z=126$ and 146 cm, the LIF intensity and by implication, the metastable Xe^+ density almost linearly decreases with increasing argon fraction. For an argon fraction of 87%, the Xe^+ LIF signal is still detectable but has decreased by more than 90% with respect to the pure xenon case. Also shown in Fig. 6(b) are the parallel Xe^+ flow speeds and the Xe^+ and system sound speeds. Deep in the source at $z=126$ cm, the Xe^+ parallel flow is subsonic and insensitive to increasing argon fraction. In contrast to the Ar^+ ivdf, which at $z=146$ cm exhibited a bimodal structure as a result of EDL formation, the Xe^+ ivdf is unimodal. Because xenon is more than three times heavier than argon, acceleration through an EDL identical to that found in the pure argon plasmas would yield a relative Xe^+ drift velocity of

$$v_{Xe^+}/v_{Ar^+} = (M_{Ar^+}/M_{Xe^+})^{1/2} = (40/131)^{1/2} \cong 1/\sqrt{3}. \qquad (6)$$

The above relationship was confirmed with the $z=126$ cm LIF measurements that evidenced a slight potential gradient of ~5 mV/cm along the axis of the system (assuming zero parallel flow speed at the downstream edge of the rf antenna). At the end of HELIX ($z=146$ cm) for a drift velocity of 8 km/s for Ar^+, Eq. (6) would predict a 4.6 km/s drift velocity for Xe^+. In spite of lower gas pressure operation, no distinct Xe^+ beam has been observed. At $z=146$ cm, the peak velocity of the unimodal Xe^+ vdf gradually increases with increasing argon percentage in the mixture, approaching the system sound speed for an argon fraction of ~60%. For an argon fraction of 87%, the Xe^+ parallel flow speed reaches 2.2 km/s. The conclusion that we may draw is that for an Ar–Xe mixture, the addition of a light mass gas (Ar) to a heavier gas (Xe) appears to increase the heavy ion axial flow velocity.

In the absence of any xenon ion beam observations, it is not possible to draw any conclusions regarding the effects of argon fraction on EDL formation, if any, in xenon plasmas. For smaller helicon sources, other groups have reported that neutral pressure is a key factor in EDL formation in heavy weight gases.[36,37] Bimodal RFEA-determined ivdfs with one component accelerated to supersonic speeds have been reported for xenon pressures of 0.07 mTorr by Charles and Boswell[38] and 0.09 mTorr by Shamrai *et al.*[39] Those pressures are one order of magnitude lower than the pressure used in these experiments. Attempts to lower the operating pressure led to unstable plasma conditions and unreliable LIF measurements.

In the absence of an EDL, it is typically assumed that as electrons stream out along the magnetic field lines in an open magnetic geometry such as HELIX-LEIA, an ambipolar electric field appears and the ions are dragged out by the ambipolar field.[24,40] The ionization of neutrals along the axis of the system, radial transport, ion-electron recombination, and neutral drag (due to ion-neutral collisions) can all modify the ion flow along the magnetic field lines. Radial transport effects are particularly important for HELIX-LEIA because for the first 60 cm of the source downstream of the rf antenna, the source walls are electrically nonconductive and for the next 90 cm the source has grounded walls. To calculate the magnitude of the axial electric field in HELIX, two sets of Xe^+ LIF data were obtained at $z=126$ and 146 cm. Instead of varying the mass flow rate, which introduces significant changes in the ion mean free path, the pressure was held constant at 1.3 mTorr for pure xenon and the input rf power was varied from 350 to 750 W. The square root of the Xe^+ LIF signal amplitude as a function of rf power is shown in Fig. 7(a). Since the electron temperature is roughly constant for the different input rf powers, the square root of LIF signal amplitude is a qualitative indicator of the trend Xe^+ density. Due to the inherent divergence of the injected laser beam and different LIF collection optics used at those two locations (larger lens diameter at $z=126$ cm), the LIF signal amplitude is smaller at $z=146$ cm. Therefore, to have a clear picture of the ion density evolution with input rf power, the LIF signals at both locations were normalized to their maximum values (corresponding to highest power level). With increasing rf power, a significant jump in ion density at 550 W is observed at both locations. This density jump corresponds to a discharge mode change from electrostatic (E mode) to inductive (H mode).[41–43] A second density jump that might be associated with an inductive to helicon (W mode) mode transition is also observed around 750 W. Langmuir probe electron density measurements show the first

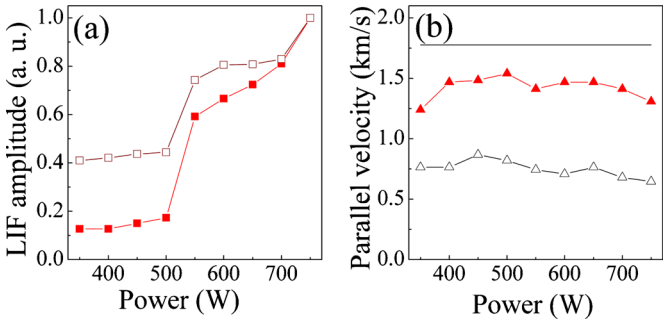

FIG. 7. (Color online) (a) Normalized Xe^+ LIF signal amplitude and (b) Xe^+ parallel flow speed vs input rf power in HELIX at $z=126$ cm (open symbols) and $z=146$ cm (filled symbols). (b) Xe^+ Bohm speed at $z=126$ cm. Operating conditions: $f=9.5$ MHz, $B_H=700$ G, $B_L=10$ G, and $p_H=1.3$ mTorr.

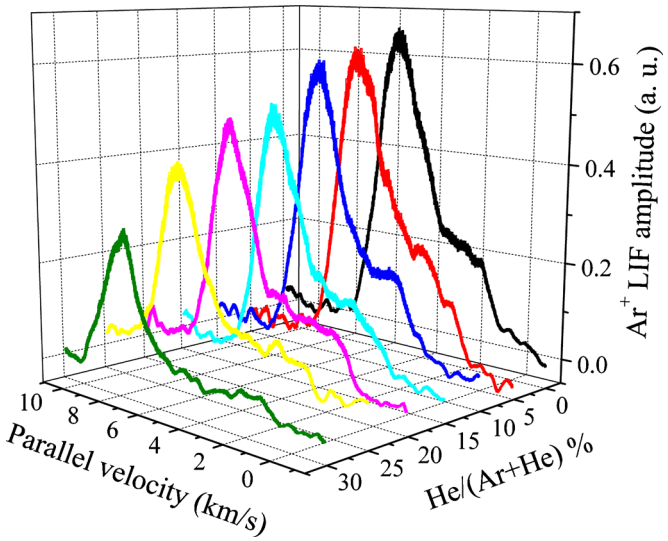

FIG. 8. (Color online) Effect of increasing helium fraction on the Ar^+ parallel ivdf in HELIX. Measurements were obtained at $z=146$ cm.

jump occurs at $\sim 5.1\times10^{10}$ cm^{-3} and the second around 1.1×10^{11} cm^{-3}. The similarity in the ion density trends at both two axial locations and the fact that more than 100 cm downstream from the antenna the LIF signal still "feels" the changes in rf coupling modes provides further support for the use of the LIF signal as a qualitative indicator of ion density. Note that these data sets were independently acquired, i.e., after the power scan was performed at $z=126$ cm, a second power scan was performed at $z=146$ cm. Thus, the matching network settings had to be completely readjusted to minimize the reflected power for both experiments. As shown in Fig. 7(b), the Xe^+ parallel flow speeds at both locations were subsonic and were not affected by changes in the rf power level. The measurements clearly show an increase in xenon ion flow speed as the ions enter in the weakening magnetic field region at the end of the source. Based on ~750 and ~1400 m/s parallel flow speeds at $z=126$ and 146 cm, respectively, and the 20 cm axial separation of the observation points, the calculated axial potential gradient is ~50 mV/cm, ten times larger than the field value obtained at $z=126$ cm from the combined Ar^+ and Xe^+ LIF measurements.

IV. ION VDFS IN Ar–He PLASMA

As described in Part I to further investigate the influence of a light mass ion on a heavier ion species velocity distribution, a series of experiments were performed in a Ar–He mixture plasma. For the sake of comparison with larger mass gas doping, the same source parameters as in the Ar–Xe plasma experiments were used: rf power of 750 W, the rf driving frequency of 9.5 MHz, HELIX magnetic field strength of 700 G, and LEIA magnetic field strength of 10 G. To modify the gas mixing ratio, helium and argon flow rates were adjusted in a controlled manner so that the total mass flow rate was kept constant at 10 SCCM. The helium fraction was only increased up to 80% because the discharge could not be maintained above 80% (at 80% the pressure in the source was 0.2 mTorr) for the chosen operating parameters, i.e., input power and magnetic field strength. For the investigated range of gas mixing ratios (0%–80% He), the argon ions dominate the plasma density [see Fig. 7(b) in Part I]. At 80% helium in the mixture, helium ions only represent 30% of the total ion population.

LIF measurements of the Ar^+ ivdf at the end of HELIX (at $z=146$ cm) for different argon-helium compositions are shown in Fig. 8. Up to helium fractions of 30%, a bimodal Ar^+ ivdf comprised of fast and slow populations is observed. For helium fractions greater than 30%, the Ar^+ LIF signal is buried in the noise and the ivdf could not be measured. The overall decrease in LIF signal (proportional to metastable Ar^+ density) and the shift toward higher speeds for the fast ion population with increasing helium fraction are immediately obvious in the measured ivdfs.

These measurements partially contradict previous Ar^+ LIF observations in an Ar–He electron cyclotron plasma by Sadeghi *et al.*[44] For a constant helium flow rate in those experiments, an increase in argon flow rate led not only to an overall decrease of the argon LIF signal but also to a decrease in the slow/fast LIF signal ratio as well. Both studies obtained the same results for the direction of the velocity shift, i.e., a reduction in the argon fraction (increase in helium fraction) leads to an increase in the parallel ion flow speed. Although the experiments differ in implementation (in our experiment the total gas flow is held constant whereas in their work the flow of one gas was held constant while the flow rate for the second gas was varied) the total pressure ranges (0.2–1.3 mTorr in our experiment versus 0.4–1 mTorr for Sadeghi's experiment) and gas composition (0%–80% helium in our work versus 33%–87% in Sadeghi's work) are similar. These quite different results for similar plasma parameters prompted a more complete analysis of the effects of increasing helium fraction on the Ar^+ ivdf.

As shown in Fig. 9(a), the total Ar^+ metastable population (obtained by integration of the LIF signal) increases with increasing argon fraction, i.e., an increase in the helium fraction yields a decrease in the overall Ar^+ LIF signal. In spite of a ~23% decrease in the total neutral pressure (from 1.3 mTorr at 0% He fraction to 1 mTorr at 30% He fraction),

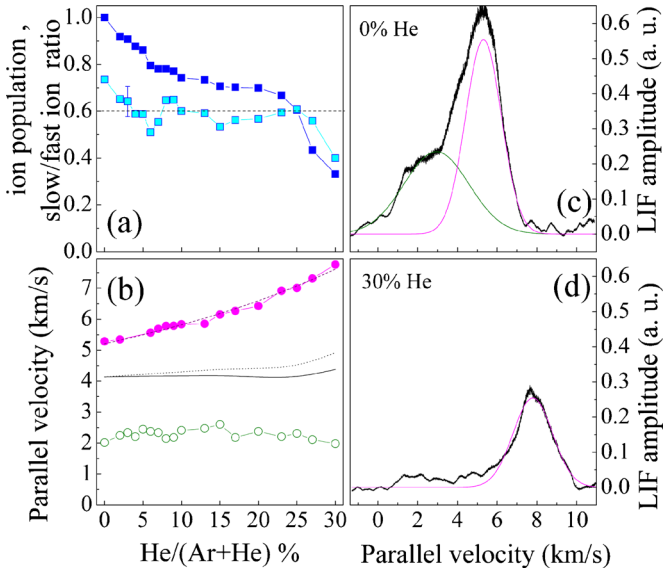

FIG. 9. (Color online) (a) Dependence of the metastable Ar^+ population obtained from integration of the ivdfs and normalized to the pure Ar case (filled squares) and ratio of slow/fast LIF Ar^+ signals (light filled squares) vs helium fraction. (b) Parallel velocity of the fast (filled circles) and slow (open circles) Ar^+ populations; the Ar^+ (solid line) and system Bohm (dotted line) speeds, respectively; the dashed line intersecting the full circles is the theoretical dependence $\sim[\alpha+\beta/(1-\gamma x)]$. (c) Bimodal ivdf with fast and slow Ar^+ populations for 0% He. (d) for a 30% He fraction the ivdf exhibits a long tail characteristic of charge-exchange collisions. Measurements obtained at $z=146$ cm in HELIX.

for helium fractions of 0%–30%, the electron temperature is roughly constant at ~7 eV [see Fig. 7(a) in Part I]. Thus, the calculated Ar^+ density suggests little variation in Ar^+ density over the same helium fraction range: a slight decrease from 1.1×10^{11} cm^{-3} in pure argon to 9.4×10^{10} cm^{-3} at a helium fraction of 25%, i.e., 15% decrease in Ar^+ density. In spite of the relative constancy of the electron temperature (which implies a constant excitation rate coefficient for the stepwise production channel of the Ar^+ 3d $^2G_{9/2}$ metastable state) and the predicted slight decrease in Ar^+ density (which implies a ~15% decrease in the Ar^+ 3d $^2G_{9/2}$ metastable state production rate), the Ar^+ LIF signal for a helium fraction of 27% is less than half (~43%) of the Ar^+ LIF signal for a helium fraction of 0% He [see Fig. 9(a)]. Because neutral helium has a number of high-energy metastable levels, e.g., 2s $^3S_1$ at 19.82 eV and 2s $^1S_0$ at 20.61 eV, other channels may contribute to populating the Ar^+ 3d $^2G_{9/2}$ state. The first such mechanism considered is Penning ionization from Ar ground state,

$$\mathrm{He}^*(2s\ ^3S_1, 2s\ ^1S_0) + \mathrm{Ar}(3p^6\ ^1S_0) \rightarrow \mathrm{He}(1s^2\ ^1S_0) + \mathrm{Ar}^+(3p^5\ ^2P^0_{3/2}).$$

Although generally efficient for our conditions, Penning ionization is unlikely to significantly contribute to the Ar^+ ground state population due to the small high-energy electron population. For helium fractions up to 30%, the eedf is clamped by argon, blocking helium excitation to higher energy levels. Furthermore, elastic collisions with helium cool the eedf and reduce the population of helium metastable levels, thereby decreasing the efficiency of the Penning ionization mechanism. A second mechanism that might increase the Ar^+ metastable population is the energy transfer process

$$\mathrm{He}^*(2s\ ^3S_1, 2s\ ^1S_0) + \mathrm{Ar}^+(3p^5\ ^2P^0_{3/2}) \rightarrow \mathrm{He}(1s^2\ ^1S_0) + \mathrm{Ar}^{+*}(3p^4 3d\ ^2G_{9/2}).$$

In spite of energy deficits for these reactions of only 0.7 and 1.5 eV (the Ar^{+*} metastable level is 19.11 eV above ion ground level), the same depleted high-energy tail of the eedf also makes this mechanism unlikely to play any role in Ar^{+*} metastable population. The decrease of the Ar^+ LIF signal could also be explained by a larger quenching cross-section of the Ar^{+*} metastable state due to collisions with ground state helium. Based on the calculated Ar^+ and He^+ relative populations and the discrepancy between the predicted Ar^+ population and LIF signal intensity, the Ar^{+*}–He quenching cross-section would have to be a factor of ~6 larger than the measured value for the Ar^{+*}–Ar quenching cross-section.[34]

Another possibility involves charge-exchange collisions that create slow ions at the expense of hot ions. At zero or low helium fraction, a deconvolution of the ivdf with two Gaussian distributions is straightforward and provides the flow speeds of the fast and slow ion groups [5.3 and 2.2 km/s for the example shown in Fig. 9(c)]. As the helium fraction increases, the fast group ivdf shifts toward higher speeds, the overall LIF detected ion population decreases and a long tail toward slower speeds replaces the well-defined slow ion group distribution [see Fig. 9(d)]. We note that similar Gaussian with long tail LIF profiles were reported in LIF ivdf observations of ions accelerated in an electrostatic presheath.[45] Therefore, the overall decrease of LIF intensity and the tail of the fast ion ivdf are most probably symptoms of a drifting distribution slowed down by elastic scattering and/or charge exchange collisions with the background gas. Assuming an Ar–Ar^+ charge-exchange cross-section[46] $\sigma_{CX}=4.7\times10^{-15}$ cm^2 for the measured ion energies gives an mfp of ~5 cm for pure argon plasma. For decreasing argon fraction, the mfp increases. It then follows that the longer tails are the result of the EDL location moving a couple of centimeters deeper in the source (as a result of the longer mfps). Fitting the distribution with only one Gaussian distribution corresponding to the fast component, integrating and then subtracting from the integral of the whole distribution, the ratio of the slow to fast ion populations can be calculated. To within errors of ~10%, the slow/fast ion population ratio is insensitive to the variations of the gas composition [see Fig. 9(a)]. Except the first and the last measurement values at helium fractions of 0% and 30%, the slow ion population density is roughly 60% of the fast ion population density (dashed horizontal line). This observation is consistent with an increasingly efficient, nonvelocity dependent quenching mechanism. In other words, as the helium fraction increases, the slow and fast Ar^{+*} metastable populations decrease at the same rate.

Perhaps the most interesting result of these investigations is the shift toward higher energies of the fast Ar^+ component as the helium fraction increases. As shown in Figs. 9(b)–9(d), increasing the helium fraction from 0% to 30% increases the parallel Ar^+ flow speed from 5.3 to 7.8 km/s. In

terms of kinetic energy, the fast Ar^+ energy increases from 5.8 to 12.6 eV. As already discussed, charge-exchange and Penning processes affect the Ar^{+*} metastable population or slow down the entire Ar^+ distribution, but do not increase the EDL strength. One possible explanation involves the decrease in the total pressure as the helium fraction increases. Sun *et al.*[7] found an empirical relationship for the parallel flow speed in pure argon plasmas,

$$v_{\parallel} = B + A/p, \tag{7}$$

where A and B are free parameters and p is the neutral pressure. From a simple model based on the momentum balance equation, they found that the EDL strength, i.e., the potential drop across the layer, increases with decreasing the neutral pressure. Since up to helium fractions of 30% the dominant ion is Ar^+, Eq. (7) should hold for Ar–He plasmas. That this model provides an accurate prediction for the Ar^+ flow speed is demonstrated in Fig. 9(c), where the experimentally determined flow velocities and the equivalent expression

$$v_{\parallel} = \alpha + \beta/(1 - \gamma x), \tag{8}$$

where α, β, and γ are free parameters and x is the helium fraction, they are shown on the same plot. One significant difference between these mixed gas experiments and the pure argon plasma results was that in pure argon plasma, the EDL strength dependence on pressure was equivalent to a dependence on the electron temperature. In these mixed Ar–He plasmas (up to helium fractions of 30%), the electron temperature does not vary, yet the ion parallel kinetic energy still doubles.

Different than other studies of ion acceleration in mixed plasmas that report an increase in the infall speed as the ions traveling through the presheath approach the sheath edge,[47,48] our measurements are happening far downstream of the "Bohm speed limit" location; the upstream EDL edge. Therefore, the model that explains ion flow speeds equal to system ion sound speed at the sheath edge in those studies is not valid for our case. Here, the ion acceleration results from the combined effects of EDL potential drop, magnetic field divergence, and geometrical expansion.

V. DISCUSSION

Ion velocity distribution functions in two ion specie plasmas were studied for two binary gas mixtures: Ar–Xe and Ar–He. In the case of Ar–Xe plasma, we found that in the source both the Ar^+ and Xe^+ ivdfs are unimodal. Their parallel speeds ($\sim$1.7 km/s for Ar^+ and $\sim$1 km/s for Xe^+) are subsonic and unaffected by the change in the gas composition. The fact that their speed ratio scales inversely proportional with ion mass ratio indicates a slight axial potential gradient. Close to the HELIX-LEIA junction at $z=146$ cm and for a very narrow range of gas composition (0%–4% xenon fraction), the argon ivdf shows a bimodal structure, indicative of an EDL upstream of the measurement location. The fast ion component has a parallel speed that linearly increases with the xenon fraction from $\sim$6.7 km/s in pure argon to $\sim$8 km/s for a 4% xenon fraction. These values are well above the argon ion or system sound speeds ($\sim$4 km/s). The slow ion component has a parallel speed of $\sim$2.5 km/s and is not affected by the small change in the gas composition. Additional ivdfs taken 1 and 2 cm downstream of the $z=146$ cm location show a slight increase in the speed of the fast group, an indicative of a second acceleration mechanism. Deep in LEIA, the bimodal character of the Ar^+ ivdf is maintained. For the narrow 0%–3% xenon fraction range for which the Ar^+ ivdf is detectable, both slow and fast ion population speeds are not affected by the change in the gas composition. As was found in pure argon, the parallel flow speed of the fast ion component ($\sim$10.5 km/s $\cong 2.6 c_{Ar+}$) is larger at $z=169$ cm than at $z=146$ cm. The $\sim$8–13 eV difference in parallel kinetic energy cannot be solely explained by radial or azimuthal kinetic energy conversion based on magnetic moment conservation. Therefore, the additional ion acceleration has to result from other mechanism(s) such as magnetic and/or geometric expansion. Although existence of the EDL is implied by the bimodal nature of the Ar^+ ivdf at $z=146$ cm, the Xe^+ ivdf is unimodal. Since the Ar^+ and Xe^+ LIF measurements do not encompass a common gas mixture range, it is possible that at moderate pressures the EDL does not form for xenon fractions above a threshold value. Previous experiments have found that in pure xenon plasma, EDL formation requires a much lower pressure ($\sim$0.07 mTorr) than in argon ($\sim$1.5 mTorr).

Because the investigated 5d $^4D_{7/2}$ Xe^+ metastable state is a relatively low energy state (11.83 eV), the Xe^+ LIF signal is detectable down to a xenon fraction of 13%. Over a xenon fraction range of 0 to 13%, the parallel flow speed slightly increased from $\sim$1.3 km/s in pure xenon to $\sim$2.2 km/s for a xenon fraction of 13%. 2.2 km/s is slightly larger than the xenon ion sound speed, but smaller than the system sound speed. If an EDL forms at the end of the plasma source in a mixed gas plasma, the kinetic energy of both species should reflect the energy gain of passing through the EDL. Although uniquely capable of identifying the behavior of each ion specie in the EDL (an RFEA is unable to distinguish between the two ion species), the lack of a fast ion component in the Xe^+ ivdf at $z=146$ cm for xenon fractions for which fast ions were observed in the Ar^+ ivdf prevented us from confirming the EDL strength implied by Ar^+ ivdf measurements.

As observed in the Ar–Xe plasma, the LIF measured Ar^+ ivdf in the Ar–He plasma at the end of the helicon source exhibits a bimodal structure with fast and slow ion populations. However, in the Ar–He plasma, the LIF signal is detectable up to helium fractions of 30%. With increasing helium fraction, the parallel flow speed of the fast Ar^+ population increased from $\sim$5.2 km/s at 0% helium fraction to $\sim$7.8 km/s at a helium fraction of 30%. As the helium fraction increased, the slow argon ion population changed from a single Gaussian to a wide distribution, extending all the way from the speed of the fast population to 0 m/s; a shape characteristic of a distribution of particles slowing down due to charge-exchange collisions. The larger Ar^+ flow speeds observed with increasing helium fraction might result from the same additional acceleration mechanism postulated to be at work in pure Ar and Ar–Xe plasmas. An effective He^+ LIF scheme would allow comparison of the Ar^+ and He^+

parallel flow speeds and provide critically needed additional information about the ion acceleration mechanisms.

ACKNOWLEDGMENTS

I.A.B thanks Dr. X. Sun now at Tri-Alpha Co., Dr. C. Biloiu now at Varian Semiconductor Equipment Associates, Dr. A. M. Keesee, and Dr. A. Hansen for many enlightening discussions, suggestions, and critical analyses regarding this work. This work was supported by NSF Award No. PHY-0611571.

[1]X. Sun, A. M. Keesee, C. Biloiu, E. E. Scime, A. Meige, C. Charles, and R. W. Boswell, Phys. Rev. Lett. **95**, 025004 (2005).
[2]E. E. Scime, I. A. Biloiu, J. Carr, Jr., S. Chakraborty Thakur, M. Galante, A. Hansen, S. Houshmandyar, A. M. Keesee, D. McCarren, S. Sears, C. Biloiu, and X. Sun, Phys. Plasmas **17**, 055701 (2010).
[3]S. Chakraborty Thakur, Z. Harvey, I. A. Biloiu, A. Hansen, R. A. Hardin, W. S. Przybysz, and E. E. Scime, Phys. Rev. Lett. **102**, 035004 (2009).
[4]I. A. Biloiu and E. E. Scime, Phys. Plasmas **17**, 113508 (2010).
[5]I. A. Biloiu, E. Scime, and C. Biloiu, Plasma Sources Sci. Technol. **18**, 025012 (2009).
[6]D. C. Zimmerman, R. McWilliams, and D. A. Edrich, Plasma Sources Sci. Technol. **14**, 581 (2005).
[7]X. Sun, C. Biloiu, R. Hardin, and E. E. Scime, Plasma Sources Sci. Technol. **13**, 359 (2004).
[8]H. Salami and A. Ross, J. Mol. Spectrosc. **233**, 157 (2005).
[9]C. J. Sansonetti, Lawrence Livermore National Laboratory Report No. UCRL-CR-125216, 1996.
[10]M. J. Goeckner and J. Goree, J. Vac. Sci. Technol. A **7**, 977 (1989).
[11]F. Skiff and J. Bollinger, Phys. Plasmas **11**, 2972 (2004).
[12]I. A. Biloiu, X. Sun, and E. Scime, Rev. Sci. Instrum. **77**, 10F301 (2006).
[13]T. Nakano, N. Sadeghi, and R. A. Gottscho, Appl. Phys. Lett. **58**, 458 (1991).
[14]G. A. Hebner and A. M. Paterson, Plasma Sources Sci. Technol. **19**, 015020 (2010).
[15]T. B. Smith, "Deconvolution of ion velocity distributions from laser-induced fluorescence spectra of xenon electrostatic thruster plumes," Ph.D. thesis, Aerospace Engineering, University of Michigan, 2003.
[16]I. A. Biloiu, E. E. Scime, and C. Biloiu, *The XIXth International Conference on Physics of Ionized Gases*, edited by J. de Urquijo, published on CD, 12 July 2009, Cancun, Mexico.
[17]See: http://physics.nist.gov/PhysRefdData/ASD?index.html for Xe^+ transition wavenumber.
[18]*CRC Handbook of Chemistry and Physics 68th Edition*, edited by R. C. Weast, M. J. Astle, and W. H. Beyer (CRC, Boca Raton, FL, 1988).
[19]C. J. Humphreys, J. Res. Natl. Bur. Stand. **22**, 19 (1939).
[20]C. J. Humphreys and E. Paul, Jr., J. Opt. Soc. Am. **60**, 1454 (1970).
[21]J. E. Hansen and W. Persson, Phys. Scr. **36**, 602 (1987).
[22]R. J. Cedolin, W. A. Hargus, Jr., P. V. Storm, R. K. Hanson, and M. A. Cappelli, Appl. Phys. B: Lasers Opt. **65**, 459 (1997).
[23]N. Sadeghi, N. Dorval, J. Bonnet, D. Pigache, C. Kadlec-Philippe, and A. Bouchoule, Proceedings of the 35th AIAA/ASM/SAE/ASEE/Joint Propulsion Conference and Exhibit, Los Angeles, 1999, AIAA Paper No. 2429.
[24]C. Charles and R. W. Boswell, Appl. Phys. Lett. **91**, 201505 (2007).
[25]I. A. Biloiu, E. E. Scime, and C. Biloiu, Appl. Phys. Lett. **92**, 191502 (2008).
[26]K. Takahashi, C. Charles, R. W. Boswell, M. A. Lieberman, and R. Hatakeyama, J. Phys. D **43**, 162001 (2010).
[27]O. Sutherland, C. Charles, N. Plihon, and R. W. Boswell, Phys. Rev. Lett. **95**, 205002 (2005).
[28]C. Biloiu, X. Sun, E. Choueiri, F. Doss, E. Scime, J. Heard, R. Spector, and D. Ventura, Plasma Sources Sci. Technol. **14**, 766 (2005).
[29]K. U. Riemann, IEEE Trans. Plasma Sci. **23**, 709 (1995).
[30]G. D. Severn, X. Wang, E. Ko, and N. Hershkowitz, Phys. Rev. Lett. **90**, 145001 (2003).
[31]R. N. Franklin, J. Phys. D **36**, 34 (2003).
[32]K. P. Giapis, N. Sadeghi, J. Margot, R. A. Gottscho, and T. C. John Lee, J. Appl. Phys. **73**, 7188 (1993).
[33]I. A. Biloiu and E. E. Scime, Appl. Phys. Lett. **95**, 051504 (2009).
[34]B. Pelissier and N. Sadeghi, Rev. Sci. Instrum. **67**, 3405 (1996).
[35]Z. Harvey, S. Chakraborty Thakur, A. Hansen, R. Hardin, W. S. Przybysz, and E. E. Scime, Rev. Sci. Instrum. **79**, 10F314 (2008).
[36]C. Charles, R. W. Boswell, and M. A. Lieberman, Appl. Phys. Lett., **89**, 261503 (2006).
[37]M. D. West, C. Charles, and R. W. Boswell, J. Phys. D **42**, 245201 (2009).
[38]C. Charles and R. W. Boswell, IEEE Trans. Plasma Sci. **36**, 2141 (2008).
[39]K. P. Shamrai, V. F. Virko, Yu. V. Virko, and K. Toki, Bull. Am. Phys. Soc. **52**, 133 (2007).
[40]J. Prager, R. Winglee, T. Ziemba, B. R. Roberson, and G. Quetin, Plasma Sources Sci. Technol. **17**, 025003 (2008).
[41]A. W. Degeling, T. E. Sheridan, and R. W. Boswell, Phys. Plasmas **6**, 3664 (1999).
[42]V. Kaeppelin, M. Carrere, and J. B. Faure, Rev. Sci. Instrum. **72**, 4377 (2001).
[43]F. F. Chen and H. Torreblanca, Plasma Sources Sci. Technol. **16**, 593 (2007).
[44]N. Sadeghi, T. Nakano, D. J. Trevor, and R. Gottscho, J. Appl. Phys. **70**, 2552 (1991).
[45]N. Claire, G. Bachet, U. Stroth, and F. Doveil, Phys. Plasmas **13**, 062103 (2006).
[46]A. V. Phelps, J. Phys. Chem. Ref. Data **20**, 557 (1991).
[47]D. Lee, G. Severn, L. Oksuz, and N. Hershkowitz, J. Phys. D **39**, 5230 (2006).
[48]X. Wang and N. Hershkowitz, Phys. Plasmas **13**, 053503 (2006).